Evaluation Index System for Environmental Restoration Effectiveness Based on Landscape Pattern and Ecological Low-Carbon Construction

Jingyuan Mao*
China Railway Eryuan Engineering Group Co., Ltd., Chengdu, Sichuan Province, 610031, China

***Abstract*—Traditional green view rate (GVR) methods, which rely on two-dimensional planar images, have several limitations. They fail to capture the three-dimensional spatial characteristics of urban greenery, are frequently dependent on subjective parameters such as camera angles and lighting, and require labor-intensive manual analysis. These factors limit the accuracy and scalability of green space assessments. To overcome these challenges, this study introduces the Panoramic Green Perception Rate (PGPR). This novel metric utilizes spherical panoramic imagery and deep learning for the automated recognition of three-dimensional vegetation. A Dilated ResNet-105 network was used, achieving a mean Intersection over Union (mIoU) of 62.53% with only a 9.17% average deviation from manual annotation. PGPR was empirically applied in Ziyang Park, Wuhan, where it effectively quantified green visibility across urban activity spaces. This approach allows for the scalable and objective evaluation of urban greenery, which has practical applications in urban planning, landscape assessment, and ecological low-carbon construction. Urban planners, environmental engineers, and computer vision and smart city development researchers will find it especially useful.**

Keywords*—Panoramic green perception rate; deep learning; urban green space; vegetation recognition; landscape assessment

I. INTRODUCTION

Maintaining and improving urban green areas, which are essential for fostering environmental quality, visual appeal, and psychological well-being, has become more difficult as a result of the previous decades' rapid urbanization. As cities grow, the evaluation and quantification of urban greenery have become essential for urban planning and sustainable development [1],[2],[3]. Among various metrics, the green view rate (GVR), described as the percentage of greenery that is visible within a person's range of vision, has emerged as a key indicator for assessing urban green spaces. Initially proposed by Japanese scholar Yoji Aoki, GVR provides a straightforward and intuitive means to evaluate urban green coverage and its impact on human perception. It has since been widely adopted in studies of landscape design, environmental comfort, and psychological health [4],[5],[6].

Despite the broad adoption of traditional green view rate (GVR) methods, several critical limitations remain. Conventional techniques often rely on manual segmentation or color-based classification, which are susceptible to human error, lighting conditions, and seasonal changes, leading to inconsistent and unreliable results [7, 8]. Furthermore, most existing studies operate on static 2D imagery, failing to capture the immersive, three-dimensional nature of human visual experience in outdoor environments [9]. Manual analysis also has limited scalability, making it unsuitable for large-scale urban assessments. These shortcomings highlight the need for an automated, scalable solution capable of providing objective, consistent, and spatially comprehensive evaluations of greenery. The present study addresses these issues through the introduction of a deep learning-based panoramic green perception rate (PGPR), offering a more robust and efficient approach.

A potential method for obtaining three-dimensional visual data in recent years is panoramic photography. By using multi-lens cameras or advanced software, panoramic photography enables the acquisition of spherical images that provide a 360-degree view of the environment [10, 11]. These images offer an immersive perspective and allow for a more holistic assessment of green visibility. Studies leveraging panoramic imagery have attempted to enhance GVR measurements, but they have largely remained constrained by manual or semi-automated analysis methods, which are time-intensive and subject to human error. Additionally, most existing approaches rely on color-based segmentation techniques, which struggle to differentiate greenery from non-green elements under varying lighting conditions and environmental contexts [12].

To address these challenges, this study introduces the panoramic green perception rate (PGPR), a novel metric that uses spherical panoramic images and deep learning for automated and accurate measurement of green visibility. Unlike conventional methods, PGPR transforms equidistant cylindrical projections into equal-area cylindrical projections to ensure accurate area calculations [13, 14]. Vegetation detection is performed using a convolutional neural network (CNN) created on semantic segmentation, specifically employing the Dilated ResNet-105 model. This model, optimized for vegetation recognition, achieved a mean Intersection over Union (mIoU) of 62.53%, with an average deviation of only 9.17% compared to manual annotations. Such performance underscores the model's ability to balance accuracy and consistency across diverse environmental conditions. Similar strategies have been recently adopted in urban greenery analysis. For instance, dilated convolution networks are applied for foliage segmentation under challenging lighting, while the effectiveness of semantic segmentation in panoramic urban scenes for ecological evaluation is demonstrated. Building on prior work in adaptive zoning and spectro-temporal

*Corresponding Author

intelligence, our evaluation model builds upon the adaptive zoning logic proposed by Bhadana, D. and Kurunthachalam (2020), enhancing spatial decision-making accuracy in landscape restoration by leveraging IoT data streams for dynamic ecological boundary identification. Similarly, Bhadana, D. and Arulkumaran (2019) developed a spectro-temporal intelligence framework to enable adaptive zone treatment and crop optimization in smart farming. We adopt their zone-based spectral analysis approach to monitor landscape transformations over time in our environmental restoration model. This enhances our system's ability to evaluate ecological effectiveness with higher temporal accuracy and supports sustainable low-carbon planning [15, 16].

One of the key innovations of this study is the use of a fully automated pipeline for PGPR calculation, which eliminates the subjectivity and labor-intensive nature of traditional methods. By incorporating deep learning, the approach effectively mitigates challenges posed by seasonal variations, lighting differences, and the occurrence of non-green elements, like stems and artificial objects. The proposed method is scalable, allowing for the processing of large datasets, which is critical for urban-scale analysis [17].

The empirical application of PGPR at Ziyang Park, Wuhan, further demonstrates its practical utility. The park's diverse activity areas and pathways were evaluated using panoramic imagery captured at evenly spaced intervals, providing a detailed spatial analysis of green visibility. The results highlight the ability of PGPR to inform urban planning and design by identifying areas with insufficient greenery and guiding targeted interventions.

Despite its advantages, the study acknowledges certain limitations. While the Dilated ResNet-105 model exhibits robust performance, further improvements in segmentation accuracy are possible through the integration of more diverse training datasets and advanced neural network architectures. Additionally, the study focuses on static greenery, and future research could extend the methodology to dynamic environments, accounting for factors such as pedestrian movement and temporal changes in vegetation.

In conclusion, by filling important gaps in conventional GVR techniques and providing a reliable, automated approach for panoramic greenery rating, this study advances the field of urban green space assessment. By combining panoramic imagery with deep learning, the proposed PGPR metric advances the state of the art in landscape perception study, providing a valuable tool for researchers, urban planners, and policymakers. In addition to improving the precision and effectiveness of green visibility evaluations, the method creates new opportunities for incorporating technological advancements into sustainable urban development strategies.

II. Calculating and Measuring Panoramic Green Visibility

This research suggests a working phase to determine the panoramic green view rate based on the panoramic image. This step includes calculating the visible vegetation area, transforming the panoramic image projection, and acquiring the panoramic image.

A. Cylindrical Projection that is Isometric to Spherical Coordinates

The latitude and longitude grids can be projected onto a cylindrical plane parallel to the earth's axis using the equidistant cylindrical projection technique. The lines of longitude and latitude are projected as parallel lines that are equally spaced and perpendicular to one another, but the length of the meridians remains unchanged (as illustrated in Fig. 1). Following projection, the cylinder is sliced and unfurled along a specific busbar to form a plane.

Fig. 1. Circular projection that is isometric.

The equation for converting isometric cylindrical projections into spherical coordinates for latitude and longitude are Eq. (1) and Eq. (2):

$$\lambda = x_1/(\cos\phi_1) + \lambda_0 \tag{1}$$

$$\phi = y_1 + \phi_1 \tag{2}$$

where, the fixed point's location in spherical coordinates is identified by its longitude (λ) and latitude (ϕ).ϕ_1 represents the standard latitude line in the spherical coordinate system, $\lambda_0$is the central longitude line, and x_1 and y_1 correspond to the horizontal and vertical coordinates of the isometric cylindrical projection, respectively. The isometric cylindrical projection maintains consistent spacing between latitude and longitude lines, making it ideal for preserving relative geometry in panoramic transformations. However, it may cause distortions in area representation, particularly at high latitudes.

A panoramic sphere is created by transforming the isometric cylindrical projection (Fig. 2).

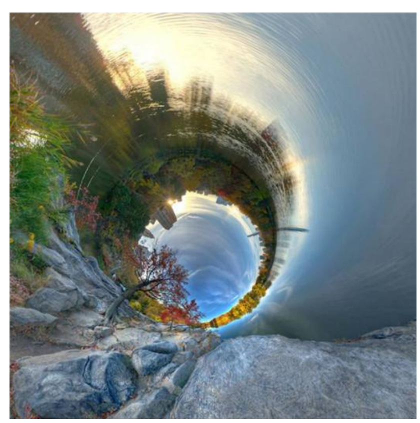

Fig. 2. The panoramic domain.

B. Equiprojected Cylindrical Projection from Spherical Coordinates

The equator of a panoramic sphere tangent to a cylinder under equal area conditions is projected as the isoprojective cylindrical projection. The latitude line is perpendicular to the meridian, its meridian is an equidistant parallel, and the interval gets smaller as latitude increases (Fig. 3).

Fig. 3. Equiprojected cylindrical projection.

Eq. (3) and Eq. (4) aims at creating an equiprobable cylindrical projection from a panoramic sphere：

$$x_2 = (\lambda - \lambda_0) \cos \lambda_0 \quad (3)$$

$$y_2 = \sin \phi \,/\, \cos \lambda_0 \quad (4)$$

λ denotes the longitude of the panoramic sphere, ϕ the latitude, λ_0 the central meridian, and x_2 and y_2 the horizontal and vertical coordinates of the isoprojective cylinders, respectively. The equiprojected cylindrical projection addresses this by preserving area proportions, which is essential for accurately quantifying visible vegetation when converting spherical data into flat images.

III. AUTOMATIC RECOGNITION

A. Features of Semantic Segmentation Neural Networks

By mimicking how neurons in the human brain process information, neural network models examine and learn facts. Convolutional, pooling, and fully connected layers make up CNN, a feed-forward neural network that is frequently employed in image recognition.

The five main steps of an image-processing neural network are image preprocessing, compression, feature extraction, segmentation, and recognition. Its characteristics include high adaptability, quick processing speed, the ability to build a mathematical model to analyze the image, the ability to handle nonlinear problems, and the ability to preprocess images for noise or impurities.

Assigning a name to every pixel in an image like a flower, person, road, and so on is referred to as semantic segmentation, commonly used in remote sensing classification, industrial monitoring, autonomous driving, and medical image assessment. Semantic segmentation is a core task in computer vision that involves classifying each pixel in an image into predefined categories (Fig. 4) . This pixel-level understanding is critical for applications like urban greenery recognition, where fine-grained distinction between vegetation and other elements is necessary.

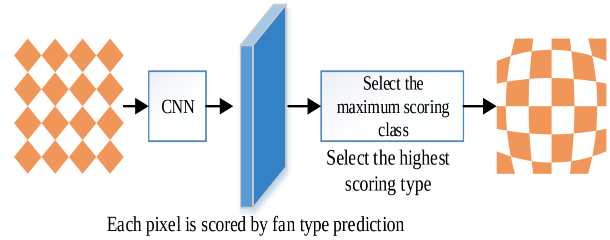

Fig. 4. Semantic segmentation of images using neural network models.

B. Models for Semantic Picture Segmentation

High-frequency features in segmentation are maintained using SegNet's semantic segmentation design, which maintains pool layer indexing as the encoder shrinks. Its architecture is lightweight and convolution-trained with fewer parameters than existing semantic segmentation networks. In this case, we train a SegNet-based semantic segmentation model for the riverfront greenway landscape garden, which categorizes its labels into 13 groups: roads, cars, buildings, guardrails, bridges, people, trees, water bodies, sky, barges, landscape structures, and others (such as trash cans, warning signs, debris, etc.).

The image semantic segmentation process (Fig. 5) proceeds as follows：

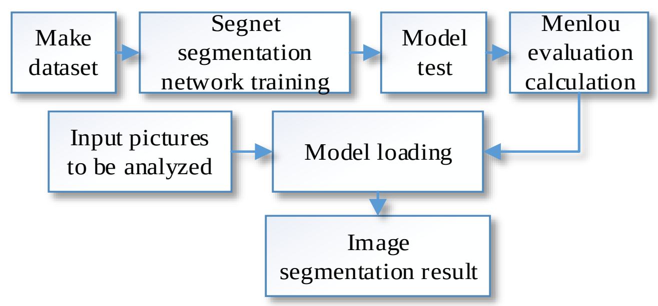

Fig. 5. Building a semantic segmentation model for a picture of a waterfront setting.

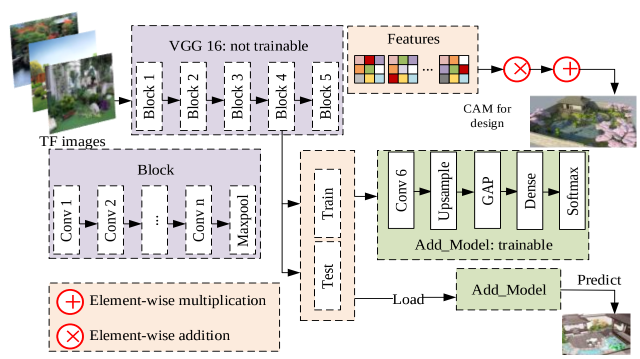

Fig. 6. Proposed semantic segmentation model architecture.

The model in this study labels and classifies the pixels, as Fig. 6 illustrates. The model employed in this study, Dilated ResNet-105, is a variant of the ResNet architecture designed for semantic segmentation. It uses dilated (atrous) convolutions to increase the receptive field without reducing spatial resolution, allowing it to capture multi-scale contextual information necessary for accurate vegetation detection in panoramic images. To create the dataset, 90 riverside panorama photos were chosen, labeled with 13 landscape components in MATLAB, and then trained using the SegNet segmentation network. Eq. (5) to Eq. (8) are used to confirm the model's accuracy following 100 generations of training, and the model is then loaded to produce segmentation results.

$$A_i = \frac{P_{ii}}{P_{ij}} \tag{5}$$

$$IoU_i = \frac{P_{ii}}{P_{ij}+P_{ji}-P_{ii}} \tag{6}$$

$$\text{PA} = \frac{\sum_{i=0}^{k} P_{ii}}{\sum_{i=0}^{k}\sum_{j=0}^{k} P_{ij}} \tag{7}$$

$$\text{MIoU} = \frac{1}{k+1}\sum_{i=0}^{k}\frac{P_{ii}}{\sum_{j=0}^{k} P_{ij}+\sum_{j=0}^{k} P_{ji}-P_{ii}} \tag{8}$$

C. Analysis of Visual Perception

Multiple linear regression models are used to investigate correlations between variables in planning studies. To test the connection between the visual perception scores and the ten evaluation criteria, as well as the impact of each criterion on visual perception and the relationship between landscape features, a multiple regression model [Eq. (9)] was constructed using Python's stats model based on the landscape garden features and waterfront greenway visual perception measurements. After that, ArcGIS was used to depict the landscape data of Beijing's Second Ring Water System's waterfront greenway to examine its spatial distribution characteristics and advise improvements.

$$y = \beta_0 + \beta_1 x_1 + \cdots + \beta_n x_n + \epsilon \tag{9}$$

where, y is the visual perception score, $\beta_0, \beta_1, \cdots, \beta_n$ is the parameter for regression, x is the impact factor and ϵ is the residual.

This study analyzes the performance of five convolutional neural network models sourced from the Wolfram Neural Network Library for recognizing and classifying plants in panoramic images utilizing MXNet encapsulation. Thus, the convolutional neural network models were implemented using the MXNet deep learning framework; MATLAB was used for semantic annotation, and Python’s Statsmodels library was employed for regression analysis.

IV. Comparing the Outcomes of Several Models

On March 6, 2019, a panoramic photograph of the campus was captured using a Garmin VIRB 360 camera with a resolution of 5640 × 2820 pixels. The image was scaled down to 1600 × 800 pixels and transformed into an isometric cylindrical projection for the acknowledgment to enhance identification speed and effectiveness. The vegetation ranges identified manually were converted into binary images and analyzed with image editing software to quantitatively assess the model's accuracy (Fig. 7).

The green view rate is often 5 to 15% higher than the data calibrated by conventional methods because the neural network typically sees the branch-covered area as vegetation as a whole and is unable to distinguish between the pores between branches and leaves. Simultaneously, the neural network was unable to detect minute voids in the vegetation, which mitigated the impact of variations in leaf form, color, and quantity during the seasons and guaranteed the consistency of the recognition outcomes.

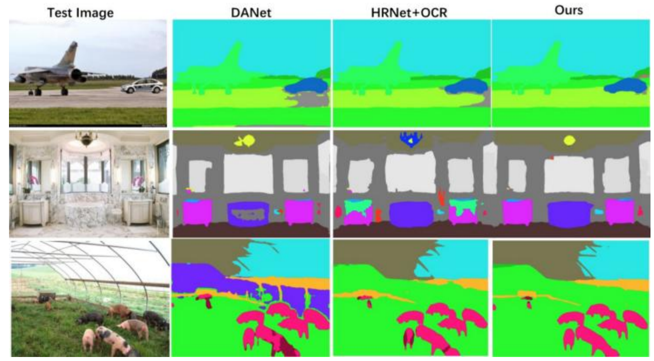

Fig. 7. Effects of several CNN models on panoramic picture recognition.

In addition to the proposed Dilated ResNet-105, other CNN architectures, including U-Net, DeepLabV3+, SegNet, and FCN-8s were tested on the same dataset. Dilated ResNet-105 had the highest mIoU (62.53%), followed by DeepLabV3+ (59.21%), U-Net (57.85%), SegNet (56.02%), and FCN-8s (54.77%). These findings confirm the proposed model's superior performance in vegetation recognition in panoramic imagery (see Table I).

TABLE I COMPARISON OF CONVOLUTIONAL NEURAL NETWORK RECOGNITION AND MANUAL RECOGNITION

Model	mIoU (%)	Green Visibility Deviation (%)	Remarks
Dilated ResNet-105	62.53	9.17	Proposed model; best performance
DeepLabV3+	59.21	10.40	Multi-scale context aggregation
U-Net	57.85	11.23	Symmetric encoder-decoder design
SegNet	56.02	12.10	Lightweight, efficient segmentation
FCN-8s	54.77	13.01	Baseline fully convolutional model

V. Measurements of Panoramic Green Visibility with Empirical Support

Ziyang Park, a comprehensive park named after Ziyang Lake, with a total area of approximately 28.0 hectares, including 11.7 hectares of water and 16.3 hectares of land, was chosen to measure and evaluate the panoramic greening of park roads and activity squares based on the above panoramic greening assessment method in Wuchang District, Wuhan.

A. Selection of Sample Points

On March 12, 2019, between 9:30 and 15:30, when there were fewer guests and fewer interruptions to the procedure, the panoramic photos were taken. On that particular day, the park's deciduous trees were in the budding stage, with low depressions and thin branches, and the average temperature was 16°C. The light was also favorable. In order to get a comprehensive view of the greenery in various activity areas, the shooting locations were chosen in an isometric manner based on the area that Ziyang Park visitors could access. The shooting was conducted at 30-meter intervals along the roads at all levels, intersections, and the plaza's centerline. Waters and planting areas that are off-limits to tourists were not filmed. Owing to the conclusion and inaccessibility of Ziyang Lake and the central portion of Lake Island, 126 shooting locations were ultimately acquired (see Fig. 8).

Fig. 8. The study's scope.

B. *Comparison of Green Vision Recognition Results*

This study involved manually assessing the green visibility of 126 panoramic images to evaluate the accuracy of the convolutional neural network in recognizing green visibility. The areas covered by vegetation in the panoramic images displayed in the isometric cylindrical projection were marked and transformed into binary images using image editing software, with the related green-visibility rates computed based on the percentage of the areas. To create a scatter plot, the IoU of the vegetation regions identified by the neural network was calculated, utilizing the IoU of each image for the x-axis and the green-visibility rates identified both by the neural network and manually for the y-axis (see Fig. 9).

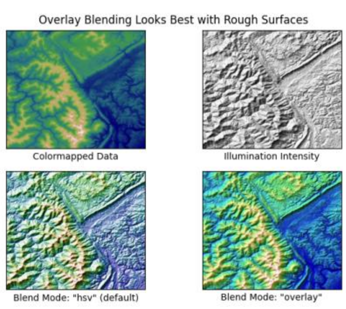

Fig. 9. Distribution of the green view rate of CNN recognition and manual recognition under different IoU.

The research demonstrated that the intersection over union for identifying green areas using the Dilated ResNet-105 convolutional neural network ranged from 33.13% to 83.68%, yielding a mean IoU (mIoU) of 62.53%. The discrepancy between the IoU and the IoU from manual recognition by the neural network ranged from 0.40% to 23.86%, with an average difference of 9.17%. A greater IoU in image recognition relates to a smaller average variance of the associated green-vision rate (see Table II).

TABLE II COMPARISON OF GREEN VISION RECOGNITION RESULTS

Low range /%	Number of panoramic photos	Percentage of panoramic photos /%	Average deviation of panoramic green viewing rate /%
30-40	3	2.38	14.15
40-50	19	15.08	13.19
50-60	23	18.25	9.92
60-70	46	36.51	8.95
70-80	29	23.02	6.66
80-90	6	4.76	4.82
Total	126	100	9.17

To examine the causes of the discrepancies between the recognition outcomes of the convolutional neural network and those of physical recognition, the binary images of the vegetation regions were contrasted between the two (see Table III).

TABLE III COMPARISON OF RECOGNITION RESULTS FOR SELECTED IMAGES

Drawing No	IoU/%	Convolution neural network recognition picture (panoramic green viewing rate /%)	Manually recognized pictures (panoramic green viewing rate /%)
1	33.13	41.85	32.7
2	44.79	44.79	43.15
3	55.24	49.51	35.54
4	65.82	49.06	38.34
5	75.41	62.89	61.11
6	83.68	40.81	41.21

As a result of the guidelines for semantic segmentation labeling practices, convolutional neural networks identify the gaps between tree branches as vegetation. Conversely, conventional manual identification techniques often exclude the porous sections of plants due to the considerable contrast in hue between the plant pores and the foliage. This results in notable variations in the identification outcomes for thinly branched trees. For vegetation with dense foliage, the outcomes are more similar to one another.

Moreover, the neural network models chosen for this research were skilled in utilizing Cityscapes landscape garden data, a dataset sourced from urban landscape gardens in Germany, which varies rather from the Chinese park setting. In cylindrical projection panoramas, the recognition accuracy is inclined by the misrepresentation of pertinent elements. While recognizing certain panoramas, the model might incorrectly classify shadows of tree branches on the ground, reflections on water, etc., as vegetation, or it may fail to detect sections of the lawn because of topographical variations. The tripod supporting the camera inevitably somewhat blocks the lower portion of the panorama while shooting, disturbing some of the outcomes.

VI. Scenic Garden Quality

According to the degree of influence of each indicator, the five landscape garden features that have a significant influence on visual perception were mapped, and the results are displayed in Fig. 10.

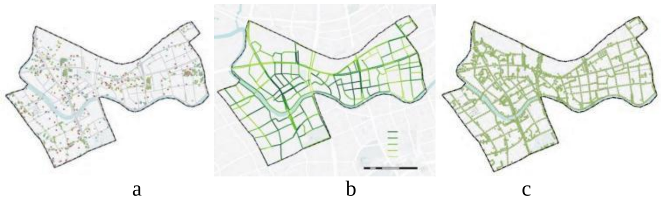

Fig. 10. Map of visual perception of scoring results with three features that had a significant impact.

Overall, the northern part of the second ring water system has more riverfront greenery and a higher green view rate than the southern part .The southern section of the Tonghui River and the moat is dominated by vertical barges on both sides of the riverfront road, with limited space for planting; the upper layer of the riverfront road in the Beijing-Mi River Diversion Channel is bermed with plants, with ample space for greening, but the existing plant layer is mainly herbaceous, with a single level and plant species and a low greening rate, resulting in poor visual effects [see Fig. 10(a)].

The natural openness of the riverfront is more uniform and better overall, with the south slightly better than the north, due to the small variation in width of the channel in the Second Ring waterway. In particular, the waterfront greenway in the northern moat and southern Changhe section is divided by vegetation from the water body, with bulky shrubs and small trees obscuring views and a lower WO, increasing the sense of confinement and oppressiveness of the waterfront walkway space [see Fig. 10 (b)].

The visibility of water bodies in the second ring water system shows a homogeneous state, but at local points, water bodies are not visible or the water surface is over-represented in the line of sight. A small number of discontinuous scenes of poor water body visibility occur in the North Moat, North Tucheng Ditch, and South Changhe River due to the vegetation barrier between the riverfront greenway and the water body; the Beijing-Mi Diversion Channel and Yongding River Diversion Channel sections have a high BVI share due to the small height difference between the riverfront greenway and the water surface and the low height of the waterfront parapet [see Fig. 10 (c)].

VII. Conclusion

This study introduces the Panoramic Green Perception Rate (PGPR), a novel metric for more accurately quantifying urban greenery visibility compared to the traditional Green View Rate (GVR), effectively addressing the limitations of 2D image assessments. By combining spherical panoramic imagery with deep learning using the Dilated ResNet-105 model, the approach achieved a mIoU of 62.53% and a low average deviation of 9.17% from manual evaluations. The method was successfully applied and validated at Ziyang Park, enabling spatially detailed and objective analysis of green space distribution. The results demonstrate that the model's scalability and robustness under varying environmental conditions, supporting broader applications in urban-scale assessments. The findings offer practical value for urban planning and sustainable development, with future work aiming to adapt the PGPR framework to dynamic environments and enhance model performance with richer datasets. A comparative evaluation confirms that the proposed model outperforms existing CNN-based segmentation approaches in terms of mIoU and green visibility estimation, underscoring its suitability for real-world urban landscape assessment.

Declarations

Funding

The authors did not receive any funding.

Conflicts of Interest

Authors do not have any conflicts.

Data Availability Statement

No datasets were generated or analyzed during the current study.

Code Availability

Not applicable.

Authors' Contributions: Jingyuan Mao is responsible for designing the framework, analyzing the performance, validating the results, writing the study, collecting the information required for the framework, providing software, critical review, and administering the process.

References

[1] M. Ergen, "Using geographical information systems to measure the accessibility of green areas in the urban center of Nevşehir, Turkey," *Urban Forestry & Urban Greening*, vol. 62, p. 127160, 2021.

[2] Y. Yang, Y. Lu, H. Yang, L. Yang, and Z. Gou, "Impact of the quality and quantity of eye-level greenery on park usage," *Urban Forestry & Urban Greening*, vol. 60, p. 127061, 2021.

[3] D. Soba, A. L. Gámez, N. Úriz, L. R. de Larrinaga, C. Gonzalez-Murua, J. M. Becerril, and I. Aranjuelo, "Foliar heavy metals and stable isotope (δ13C, δ15N) profiles as reliable urban pollution biomonitoring tools," *Urban Forestry & Urban Greening*, vol. 57, p. 126918, 2021.

[4] T. Hu, D. Wei, Y. Su, X. Wang, J. Zhang, X. Sun, and Q. Guo, "Quantifying the shape of urban street trees and evaluating its influence on their aesthetic functions based on mobile LiDAR data," *ISPRS J. Photogramm. Remote Sens.*, vol. 184, pp. 203–214, 2022.

[5] K. Jessup, S. S. Parker, J. M. Randall, B. S. Cohen, R. Roderick-Jones, S. Ganguly, and J. Sourial, "Planting stormwater solutions: A methodology for siting nature-based solutions for pollution capture, habitat enhancement, and multiple health benefits," *Urban Forestry & Urban Greening*, vol. 64, p. 127300, 2021.

[6] C. Zhang, M. Li, and D. Wu, "Federated multidomain learning with graph ensemble autoencoder GMM for emotion recognition," *IEEE Trans. Intell. Transp. Syst.*, vol. 24, no. 7, pp. 7631–7641, 2022.

[7] C. Guan, J. Song, M. Keith, B. Zhang, Y. Akiyama, L. Da, and T. Sato, "Seasonal variations of park visitor volume and park service area in Tokyo: A mixed-method approach combining big data and field observations," *Urban Forestry & Urban Greening*, vol. 58, p. 126973, 2021.

[8] L. Langsetmo, A. M. Kats, P. M. Cawthon, J. A. Cauley, T. N. Vo, B. C.

Taylor, and the Osteoporotic Fractures in Men (MrOS) Study Group, “The association between objectively measured physical activity and subsequent health care utilization in older men,” *J. Gerontol. A Biol. Sci. Med. Sci.*, vol. 74, no. 6, pp. 820–826, 2019.

[9] Y. Ye and H. Qiu, “Environmental and social benefits, and their coupling coordination in urban wetland parks,” *Urban Forestry & Urban Greening*, vol. 60, p. 127043, 2021.

[10] W. Wu, Y. Yun, B. Hu, Y. Sun, and Y. Xiao, “Greenness, perceived pollution hazards and subjective wellbeing: Evidence from China,” *Urban Forestry & Urban Greening*, vol. 56, p. 126796, 2020.

[11] D. Wu, C. Zhang, L. Ji, Y. Zhang, and F. Liu, “Forest fire recognition based on feature extraction from multi-view images,” *Traitement du Signal*, vol. 38, no. 3, pp. 775–783, 2021.

[12] H. Li, H. Xie, and G. Woodward, “Soundscape components, perceptions, and EEG reactions in typical mountainous urban parks,” *Urban Forestry & Urban Greening*, vol. 64, p. 127269, 2021.

[13] L. Soininen, M. Grönroos, M. I. Roslund, and A. Sinkkonen, “Long-term storage affects resource availability and occurrence of bacterial taxa linked to pollutant degradation and human health in landscaping materials,” *Urban Forestry & Urban Greening*, vol. 60, p. 127065, 2021.

[14] R. Kemker, C. Salvaggio, and C. Kanan, “Algorithms for semantic segmentation of multispectral remote sensing imagery using deep learning,” *ISPRS J. Photogramm. Remote Sens.*, vol. 145, pp. 60–77, 2018.

[15] D. Bhadana and A. Kurunthachalam, “Geo-cognitive smart farming: An IoT-driven adaptive zoning and optimization framework for genotype-aware precision agriculture,” *Int. J. Commerce IT Soc. Sci*., vol. 7, no. 4, pp. 5–12, 2020.

[16] D. Bhadana and G. Arulkumaran, “STAMS-enabled genomic smart farming: A spectrotemporal intelligence framework for adaptive zone treatment and crop optimization,” *Int. J. Eng. Technol. Res*. Manag., vol. 3, no. 6, pp. 2456–9348, 2019.

[17] B. Zhao, J. Feng, X. Wu, and S. Yan, “A survey on deep learning-based fine-grained object classification and semantic segmentation,” *Int. J. Autom. Comput.*, vol. 14, no. 2, pp. 119–135, 2017.